Available online at www.sciencedirect.com

SciVerse ScienceDirect

Ceramics International 39 (2013) 6497–6502

CERAMICS INTERNATIONAL

www.elsevier.com/locate/ceramint

Growth and characterization of the Al-doped and Al–Sn co-doped ZnO nanostructures

Xinlong Tian[a], Zhanchang Pan[a,*], Huangchu Zhang[b], Hong Fan[a], Xiangfu Zeng[b], Chumin Xiao[a], Guanghui Hu[a], Zhigang Wei[a]

[a]School of Chemical Engineering and Light Industry, Guangdong University of Technology, Guangzhou, Guangdong 510006, China
[b]Victory Giant Technology (Hui Zhou) Co., Ltd., Huizhou 516083, China

Received 17 January 2013; received in revised form 26 January 2013; accepted 27 January 2013
Available online 1 February 2013

Abstract

In the present work, well-dispersed structures of spherical-like pure ZnO, Al doped ZnO (AZO) and Al, Sn co-doped ZnO (ATZO) nanocrystals were successfully synthesized by using zinc acetate dihydrate as the starting material and also the low temperature hydrothermal process without any additional surfactant or catalytic agent. The ZnO structures were characterized by X-ray diffraction (XRD), and transmission electron microscopy (TEM). The XRD results revealed that ZnO powders have a hexagonal crystal structure and the TEM indicated that the nanoparticles self-aggregate. An X-ray photoelectron spectroscopy (XPS) study confirmed the substitution of Zn^{2+} by Sn and Al ions. Optical properties of the ZnO structures were investigated by Raman spectroscopy and room-temperature photoluminescence (PL) spectroscopy. The Raman spectroscopy results demonstrated that the doped ZnO nanoparticles had a higher crystalline quality than that of pure ZnO. Room-temperature PL spectra of these structures showed a strong UV emission peak and a relative weak green emission peak, and the UV peak of the doped ZnO nanoparticles was blue-shifted with respect to that of the undoped ZnO nanoparticles.

Keywords: Al–Sn co-doped ZnO; XPS; Optical band gap; Hydrothermal

1. Introduction

Due to its unique optical, electrical, magnetic, acoustic and chemical properties, zinc oxide (ZnO) nanoparticles are a promising candidate for application in piezoelectric, optoelectronics, chemical sensors and solar cells [1–3]. Apart from the technological significance of the ZnO nanostructures, their quasi-one-dimensional structure with diameters in the range of tens to hundreds of nanometers makes them interesting from a scientific point of view. In this size range, they are expected to possess interesting physical properties and pronounced coupling quite different from their bulky counterpart [4].

Recently, a variety of methods have been introduced to prepare ZnO nanoparticles such as radio frequency sputtering [5], pulsed laser deposition [6], laser molecular beam epitaxy [7], chemical vapor deposition [8], sol–gel processing [9] and hydrothermal method [10–13]. The hydrothermal method is a promising one for fabricating ideal structures with special morphology because of the advantages such as low cost, low temperature, high yield and scalable process.

To modify structural, optical and other properties of ZnO nanostructures, it is practical to dope or decorate ZnO with other elements. In single-doped ZnO, Al doped ZnO thin films have attracted most of the researchers' attention for their several advantages in terms of conductivity, thermal and chemical stability [14–16], while Sn doped ZnO (TZO) thin films were reported for their improvement in electrical conductivity and the enhancement of green band emission [17,18]. What is more, Zn can be easily substituted by Sn ions without introducing a large

*Corresponding author. Tel.: +86 13 610193932; fax: +86 20 39322767.
E-mail addresses: tianxinlong2010@163.com (X. Tian), panzhanchang@163.com (Z. Pan), qhxy123@126.com (G. Hu).

0272-8842/$ - see front matter © 2013 Elsevier Ltd and Techna Group S.r.l. All rights reserved.
http://dx.doi.org/10.1016/j.ceramint.2013.01.081

lattice distortion due to their almost equal radius (Zn^{2+} is 0.074 nm and Sn^{4+} is 0.069 nm). There are several reports related to Al and X (In, Ga, V) co-doped ZnO thin films, such as Al–In co-doped ZnO thin films had better conductivity than Al single-doped ZnO (AZO) [19]. Al–V co-doped ZnO thin films improved the thermal stability [20] and Al–Ga co-doped ZnO thin films enhanced the humidity durability as compared with AZO [21]. Therefore, it appears that Al and Sn co-doped ZnO can be attractive because the co-doping may be leading to improvement in some properties of ZnO nanoparticles. In this paper, undoped ZnO, AZO and ATZO nanoparticles were synthesized by hydrothermal method and the structure, surface morphology and optical properties of these nanoparticles were investigated.

2. Experimental details

All chemicals for this research were of analytical grade and used without further purification. AZO nanoparticles were synthesized by dissolving 1.76 g zinc acetate dihydrate ($Zn(CH_3COO)_2 \cdot 2H_2O$, 8 mmol) and 0.097 g aluminum chloride hexahydrate ($AlCl_3 \cdot 6H_2O$, 0.4 mmol) in 40 ml deionized (DI) water ($Al^{3+}/Zn^{2+} = 5\%$). The diethylamine (8 mmol dissolved in 10 ml DI water) was added dropwise to the reaction mixture under continuous stirring for 3 h. The pH of the solution was maintained at 12.5 by 0.1 M sodium hydroxide (NaOH). The resultant mixture was transferred into Teflon lined stainless steel autoclave (100 ml) and kept at 140 °C for 3 h. The obtained precipitates were washed three times by DI and ethanol and dried at 60 °C in air, and then the obtained AZO powder was annealed at 500 °C for 1 h in a muffle furnace. For the synthesis of ATZO nanoparticles, the same materials and conditions were used except for the addition of tin tetrachloride pentahydrate ($SnCl_4 \cdot 5H_2O$, 0.07 g, 0.2 mmol) and the amount of Al was changed from 0.4 mmol to 0.2 mmol ($Al^{3+}/Zn^{2+} = 2.5\%$, $Sn^{4+}/Zn^{2+} = 2.5\%$). The undoped ZnO nanocrystals were synthesized by adopting the same procedure but without $AlCl_3 \cdot 6H_2O$ and $SnCl_4 \cdot 5H_2O$.

The crystal structural and morphological studies of the prepared ZnO and doped ZnO nanoparticles were performed by X-ray diffractometer ($\lambda = 1.5405$ Å, Rigaku-Ultima III) in the Bragg angle ranging between 10° and 70° and transmission electron microscopy (TEM, JEM JEOL 2100). The chemical state of the dopants of co-doped thin films was investigated by X-ray photoelectron spectroscopy (XPS, ESCA LAB 220-XL). The optical properties were measured by Raman spectrum (Raman microscope, Renishaw, 514.5 nm) and the room temperature photoluminescence spectrometer (PL, He–Cd Laser, 325 nm).

3. Results and discussion

Fig. 1 shows the XRD patterns of undoped and doped ZnO nanostructures. The positions of the diffraction peaks

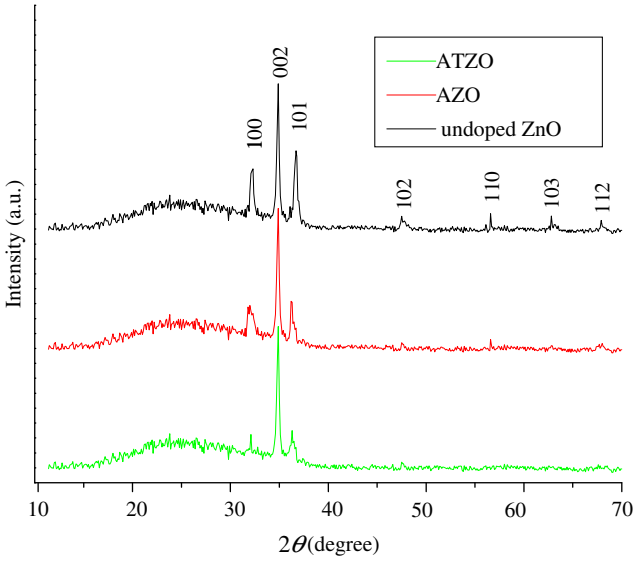

Fig. 1. XRD patterns of undoped ZnO, AZO and ATZO nanoparticles.

showed that all the films were polycrystalline with a structure that belonged to the ZnO hexagonal wurtzite type (JCPDS no. 36-1451). The absence of Sn, SnO, SnO_2 or Al_2O_3 peak excludes the existence of Al or Sn-based clusters. The higher intensity of the (002) diffraction peak compared with the(100) and (101) plane suggested that the nanoparticles exhibited a *c*-axis preferred orientation, and the *c*-axis preferred orientation was enhanced by doping. The full width at half maximum (FWHM) of the (002) plane of ATZO nanoparticles was smaller than that of undoped ZnO and AZO nanoparticles, indicating the bigger grain size of ATZO nanoparticles.

The TEM images of undoped and doped ZnO nanoparticles are shown in Fig. 2. From the TEM micrographs, it is observed that the doping has little influence on the morphological characterizations. The TEM micrographs showed that both undoped and doped ZnO nanocrystals were self-aggregated towards superstructures during the process of synthesis, which was similar to the Mn–Sn co-doped ZnO thin films reported previously [22].

Fig. 3a shows the XPS survey scan spectrum of undoped and doped ZnO nanoparticles, which was calibrated by taking the C (1s) peak (284.8 eV) as reference. Obvious Zn 2p, O 1s, and Sn 3d peaks can be seen, indicating the existence of zinc, tin and oxygen on the surface of the nanoparticles. The inset image of Fig. 3a shows the peaks corresponding to Sn $3d_{5/2}$ and the peaks consist of two oxide peaks have binding energies centered at 486.2 and 487.3 eV, which were consistent with the standard values of SnO at 486.4 eV and SnO_2 at 487.3 eV, respectively, as given in the literature [17]. The appearance of these peaks indicates the incorporation of Sn dopant in the ZnO lattice.

The Al 2p spectra of the AZO and ATZO thin films were a little weak. However, it was still successfully monitored and is shown in Fig. 3b, which can be Gaussian-resolved with three peaks centered at 72.7, 73.7 and 74.4 eV.

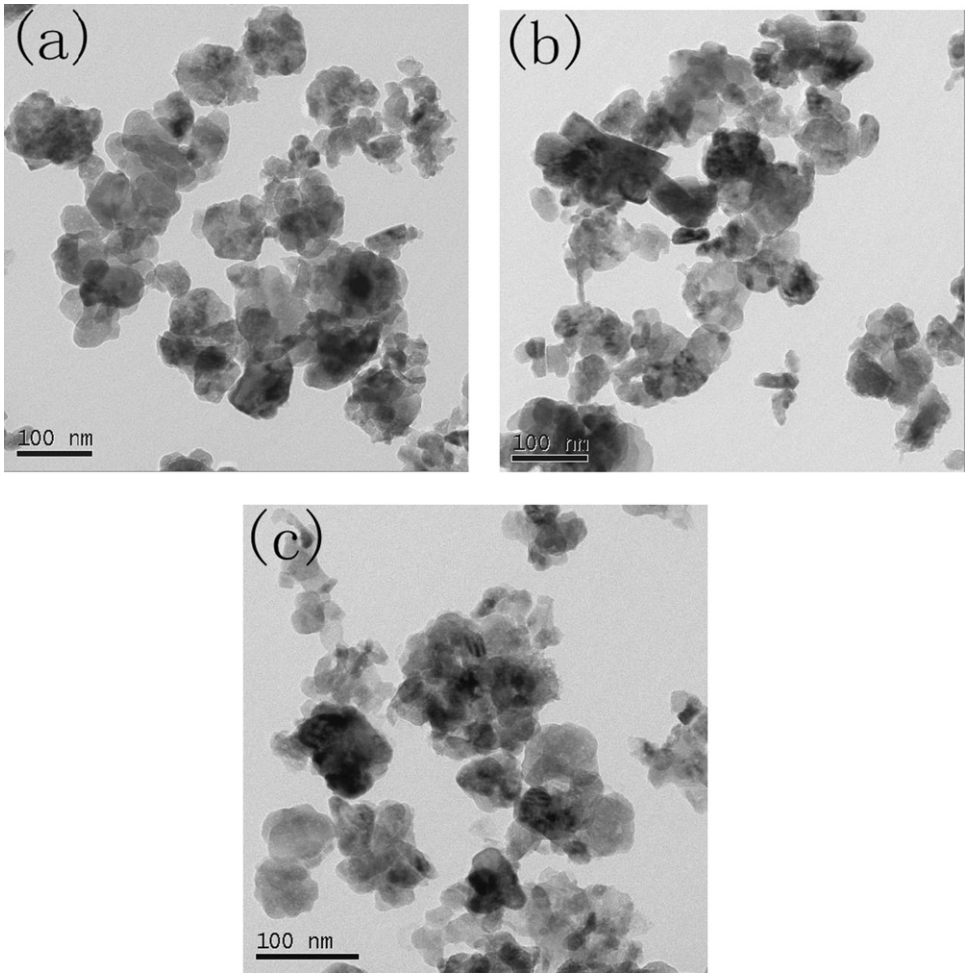

Fig. 2. TEM images of (a) undoped ZnO, (b) AZO and (c) ATZO nanoparticles.

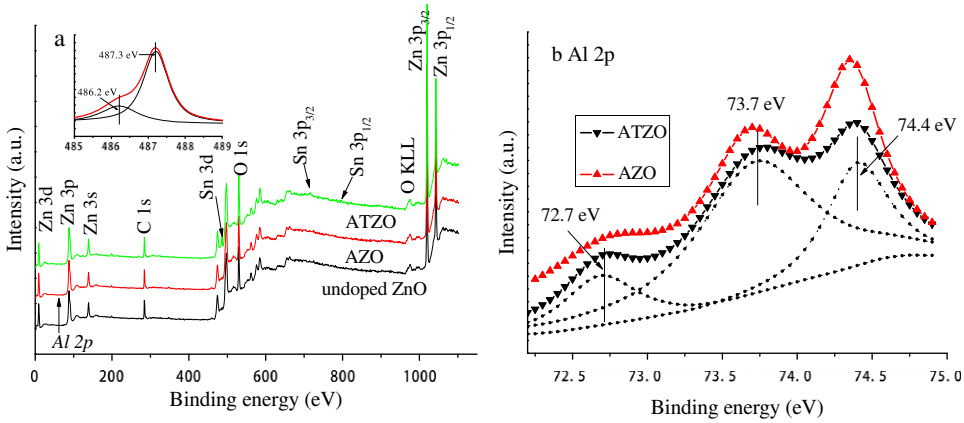

Fig. 3. (a) XPS survey scans spectra of undoped ZnO, AZO and ATZO nanoparticles (inset: XPS spectra of Sn $3d_{5/2}$), and (b) XPS spectra of Al 2p of AZO and ATZO nanoparticles.

The binding energies of 72.7 and 73.5 eV are consistent with the standard values of Al $2p_{3/2}$ and Al $2p_{1/2}$. The value of 74.4 eV, which was lower than the binding energy (75.6 eV) of amorphous Al_2O_3 films may be due to the changes of Al-surrounded atoms in different lattices [23]. The higher intensity of Al 2p spectra of AZO nanoparticles than that of ATZO was due its high Al doping concentration.

The Gaussian-resolved result for all O 1s XPS spectra in Fig. 4 shows three components of oxygen varying in chemical states which are different in binding energy O_I:

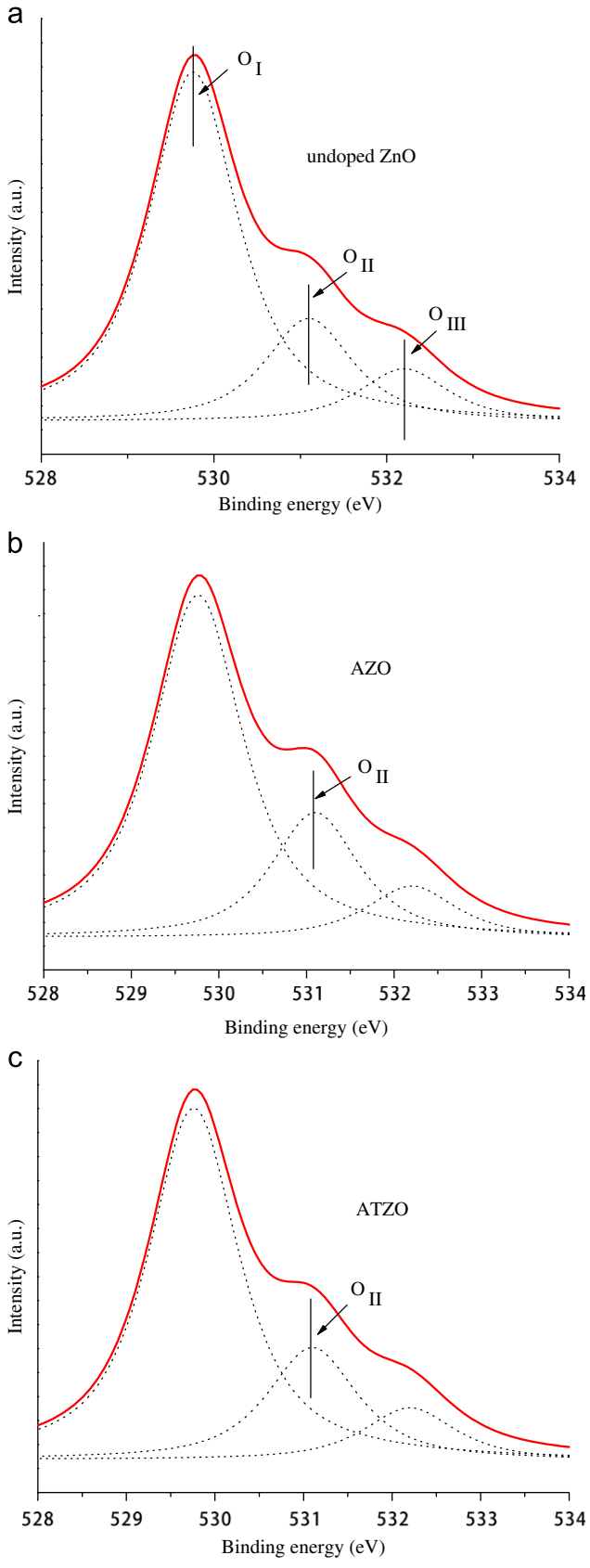

Fig. 4. XPS spectra of O 1s peak of (a) undoped ZnO, (b) AZO and (c) ATZO nanoparticles.

529.7 ± 0.15 eV, O_{II}: 531.2 ± 0.15 eV, O_{III}: 532.3 ± 0.10 eV. The highest O_{III} peak is generally ascribed to the chemisorbed oxygen at grain boundaries on the surface of the films. The lowest O_I peak is attributed to the lattice O^{2-} in the wurtzite structure of hexagonal Zn ion array. While the O_{II} peak is associated with O^{2-} in the oxygen deficient regions within the matrix of ZnO [3,10,24]. Intensity change of this peak revealed a variation of the oxygen vacancies in the films. The increment of oxygen vacancies was observed for doped ZnO nanoparticles, indicating that the level of oxygen vacancies increased with doping. In addition, the AZO nanoparticles exhibited higher level of oxygen vacancies compared with undoped ZnO and ATZO nanoparticles.

Raman spectroscopy is an effective technique for estimating the crystallinity of materials. According to the group theory, single crystalline ZnO belongs to the C_{6V}^4 space group having two formula units per primitive cell, and eight sets of optical phonon modes at the Γ point of the Brillouin zone, classified as $A_1+E_1+2E_2$ (Raman active), $2B_1$ modes (Raman silent) and A_1+E_1 modes (infrared active). The E_1 and A_1 modes are two polar modes and are split into transverse optical (TO) and longitudinal optical (LO) branches [25,26]. As shown in Fig. 5, both undoped and doped ZnO nanoparticles showed sharp, strong and dominating peaks around 437 cm^{-1}, which belongs to E_2 (high) mode of wurtzite hexagonal phase of ZnO. The peak centered at 331 cm^{-1} belonged to E_2 (low) mode. A weak peak at 583 cm^{-1} corresponding to E_1 (LO) mode was observed for the undoped and doped ZnO nanoparticles. The E_1(LO) mode is associated with impurities and formation of defects such as oxygen vacancies and Zn interstitial [10,25]. The negligible peak showed that the level of defect concentration of undoped and doped ZnO nanoparticles was very low, indicating the good crystallinity of the nanoparticles.

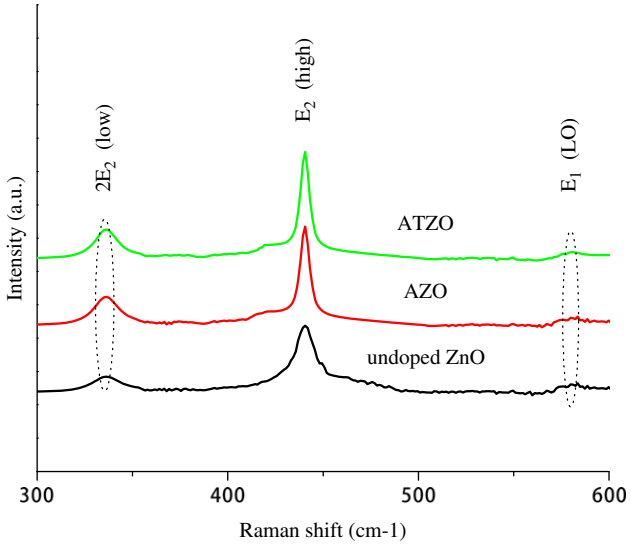

Fig. 5. Raman spectra of undoped ZnO, AZO and ATZO nanoparticles.

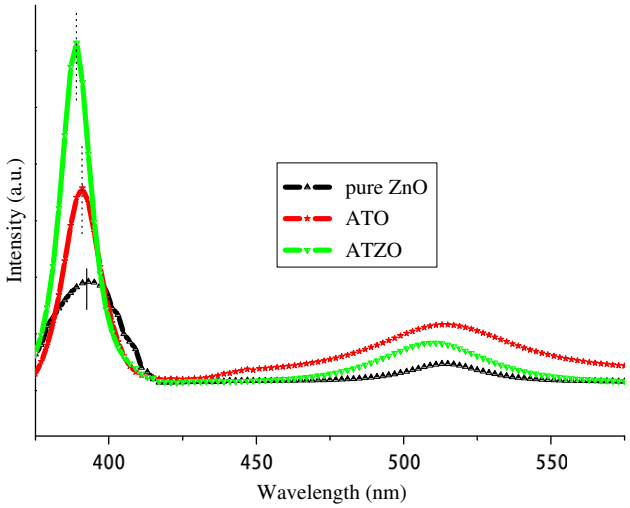

Fig. 6. PL spectra of undoped and doped ZnO nanoparticles.

Photoluminescence (PL) study is also a powerful method for investigating the effects of impurity doping on optical properties of semiconductor nanostructures with direct band gap, because doped nanostructures are expected to have different optical properties compared to undoped nanostructures [27]. Fig. 6 shows the PL spectra of the undoped and doped ZnO nanoparticles excited by 325 nm at room temperature. There are two main emission bands in the spectra, one purple peak located at about 390 nm and one broad green peak located at about 510 nm. The purple emission peak originated from excitonic recombination corresponding to the near-band-edge (NBE) emission of ZnO [10,17,26]. Compared with the undoped ZnO nanoparticles, the PL spectra of the doped ZnO nanostructures show an obvious blue shift in the UV emission (Fig. 6). This blue shift in the UV emission is believed to be a result of the Burstein–Moss effect because of the doping [28]. For doped nanocrystals, more free electrons contributed by Al and Sn dopants would take up the energy levels located at the bottom of the conduction band. When they were excited, the excitons would take up higher-energy levels at the bottom of conduction band. Radioactive recombination of these excitons will lead to a blue shift of purple emission peak [29].

The green emission peak was commonly referred to the deep-level emission (DLE), which probably relates to the transition between complex oxygen vacancy and interstitial zinc and valence band [25,26]. Slight increase of oxygen vacancies (Fig. 4) was observed in this work, so the green peaks became stronger for doped ZnO nanoparticles. The intensity ratio of I_{NBE}/I_{DLE} is regarded as an indicator of the crystal quality and optical properties of ZnO materials. The higher the ratio, the better the optical property is [27]. The increased ratio suggested that the crystal quality of doped nanoparticles were better than undoped ZnO nanoparticles, and the ATZO nanoparticles exhibited the highest ratio. The main reason to obtain these results could be the ionic radii difference. Although the doping enhanced the *c*-axis preferred orientation, the ionic radii difference between Al^{3+} (0.053 nm) and Zn^{2+} (0.072 nm) was bigger than that of Sn^{4+} (0.069 nm) and Zn^{2+} (0.072 nm). The incorporation with bigger difference of ionic radius into lattice will bring more lattice stress and lattice deformation. This effect influences the energy band structure of the ZnO nanoparticles, and as a result, new defects such as lattice distortion can be introduced by the new band structure deformation.

4. Conclusions

The simple hydrothermal method is used for preparing the undoped and doped ZnO nanoparticles. The doping significantly alters the morphology and grain size of ZnO nanoparticles. The TEM images indicated that the nanoparticles are self-aggregated to form a superstructure and XPS studies claimed the substitution of Zn ions by Sn and Al ions. The Raman spectrum showed that both the undoped and doped ZnO nanoparticles presented a good crystallinity with only a very low level of defects. What is more, the PL results showed that the optical qualities of ZnO nanoparticles were enhanced by doping and the ATZO nanoparticles were better than AZO nanoparticles under the same total doping mole ratio, which was mainly due to the lattice deformation introduced by larger ionic radii differences. In addition, the UV peaks of the PL spectra were blue-shifted for the doped samples. This indicated that doping induced the Burstein–Moss effect and band gap widening in the ZnO nanostructures.

Acknowledgments

This research was financially supported by the National Natural Science Foundation of China (20803014), Scientific and Technological Projects in Guangdong Province (No. 2012B010200035), Huizhou Daya Bay Technological Projects (20110111) and the 211 Funding Program of Guangdong Province.

References

[1] R. Yousefi, A.K. Zak, F. Jamali-Sheini, The effect of group-I elements on the structural and optical properties of ZnO nanoparticles, Ceramics International 39 (2013) 1371–1377.
[2] X. Zi-qiang, D. Hong, L. Yan, C. Hang, Al-doping effects on structure, electrical and optical properties of *c*-axis-orientated ZnO:Al thin films, Materials Science in Semiconductor Processing 9 (2006) 132–135.
[3] Z. Pan, X. Tian, S. Wu, C. Xiao, Z. Li, J. Deng, G. Hu, Z. Wei, Effects of Al and Sn dopants on the structural and optical properties of ZnO thin films, Superlattices and Microstructures 54 (2013) 107–117.
[4] M. Law, J. Goldberger, P. Yang, Semiconductor nanowires and nanotubes, Annual Review of Materials Research 34 (2004) 83.
[5] P. Carreras, A. Antony, F. Rojas, J. Bertomeu, Electrical and optical properties of Zn–In–Sn–O transparent conducting thin films, Thin Solid Films 520 (2011) 1223–1227.

[6] Y. Caglar, S. Aksoy, S. Ilican, M. Caglar, Crystalline structure and morphological properties of undoped and Sn doped ZnO thin films, Superlattices and Microstructures 46 (2009) 469–475.
[7] C.K. Ong, S.J. Wang, In situ RHEED monitor of the growth of epitaxial anatase TiO_2 thin films, Applied Surface Science 185 (2001) 47–51.
[8] C. Satriano, M.E. Fragalà, Y. Aleeva, Ultrathin and nanostructured ZnO-based films for fluorescence biosensing applications, Journal of Colloid and Interface Science 365 (2012) 90–96.
[9] Z. Pan, X. Tian, S. Wu, X. Yu, Z. Li, J. Deng, C. Xiao, G. Hu, Z. Wei, Investigation of structural, optical and electronic properties in Al–Sn co-doped ZnO thin films, Applied Surface Science 265 (2013) 870–877.
[10] S. Ameen, M.S. Akhtar, H.-K. Seo, Y.S. Kim, H.S. Shin, Influence of Sn doping on ZnO nanostructures from nanoparticles to spindle shape and their photoelectrochemical properties for dye sensitized solar cells, Chemical Engineering Journal 187 (2012) 351–356.
[11] N. Kiomarsipour, R. Shoja Razavi, Hydrothermal synthesis and optical property of scale- and spindle-like ZnO, Ceramics International 39 (2013) 813–818.
[12] R. Shi, P. Yang, X. Dong, Q. Ma, A. Zhang, Growth of flower-like ZnO on ZnO nanorod arrays created on zinc substrate through low-temperature hydrothermal synthesis, Applied Surface Science 264 (2013) 162–170.
[13] H.-G. Chen, H.-D. Lian, S.-P. Hung, C.-F. Wang, Epitaxial growth of self-ordered ZnO nanostructures on sapphire substrates by seed-assisted hydrothermal growth, Journal of Crystal Growth 362 (2013) 231–234.
[14] J.J. Ding, H.X. Chen, S.Y. Ma, The Al-doping and post-annealing treatment effects on the structural and optical properties of ZnO:Al thin films deposited on Si substrate, Applied Surface Science 256 (2010) 4304–4309.
[15] E. Bacaksiz, S. Aksu, S. Yılmaz, M. Parlak, M. Altunbaş, Structural, optical and electrical properties of Al-doped ZnO microrods prepared by spray pyrolysis, Thin Solid Films 518 (2010) 4076–4080.
[16] M. Mazilu, N. Tigau, V. Musat, Optical properties of undoped and Al-doped ZnO nanostructures grown from aqueous solution on glass substrate, Optical Materials 34 (2012) 1833–1838.
[17] M. Jung, S. Kim, S. Ju, Enhancement of green emission from Sn-doped ZnO nanowires, Optical Materials 33 (2011) 280–283.
[18] C.-Y. Tsay, H.-C. Cheng, Y.-T. Tung, W.-H. Tuan, C.-K. Lin, Effect of Sn-doped on microstructural and optical properties of ZnO thin films deposited by sol–gel method, Thin Solid Films 517 (2008) 1032–1036.
[19] T.V. Vimalkumar, N. Poornima, K.B. Jinesh, C.S. Kartha, K.P. Vijayakumar, On single doping and co-doping of spray pyrolysed ZnO films: structural, electrical and optical characterization, Applied Surface Science 257 (2011) 8334–8340.
[20] S. Suzuki, T. Miyata, M. Ishii, T. Minami, Transparent conducting V-co-doped AZO thin films prepared by magnetron sputtering, Thin Solid Films 434 (2003) 14–19.
[21] W. Lee, S. Shin, D.-R. Jung, J. Kim, C. Nahm, T. Moon, B. Park, Investigation of electronic and optical properties in Al Ga codoped ZnO thin films, Current Applied Physics 12 (2012) 628–631.
[22] K.C. Barick, M. Aslam, V.P. Dravid, D. Bahadur, Controlled fabrication of oriented co-doped ZnO clustered nanoassemblies, Journal of Colloid and Interface Science 349 (2010) 19–26.
[23] Y.-S. Kim, W.-P. Tai, Electrical and optical properties of Al-doped ZnO thin films by sol–gel process, Applied Surface Science 253 (2007) 4911–4916.
[24] S. Aksoy, Y. Caglar, S. Ilican, M. Caglar, Sol–gel derived Li–Mg co-doped ZnO films: preparation and characterization via XRD, XPS, FESEM, Journal of Alloys and Compounds 512 (2012) 171–178.
[25] R. Yousefi, F. Jamali-Sheini, Effect of chlorine ion concentration on morphology and optical properties of Cl-doped ZnO nanostructures, Ceramics International 38 (2012) 5821–5825.
[26] J. Yang, M. Gao, L. Yang, Y. Zhang, J. Lang, D. Wang, Y. Wang, H. Liu, H. Fan, Low-temperature growth and optical properties of Ce-doped ZnO nanorods, Applied Surface Science 255 (2008) 2646–2650.
[27] R. Yousefi, F. Jamali-Sheini, A. Khorsand Zak, M.R. Mahmoudian, Effect of indium concentration on morphology and optical properties of In-doped ZnO nanostructures, Ceramics International 38 (2012) 6295–6301.
[28] J. Sengupta, R.K. Sahoo, C.D. Mukherjee, Effect of annealing on the structural, topographical and optical properties of sol–gel derived ZnO and AZO thin films, Materials Letters 83 (2012) 84–87.
[29] B. Houng, H.B. Chen, Investigation of AlF_3 doped ZnO thin films prepared by RF magnetron sputtering, Ceramics International 38 (2012) 801–809.